



Cite this: DOI: 10.1039/c5ce00087d

# New topological 3D copper(II) coordination networks: catechol oxidation catalysis and solvent adsorption *via* porous properties†

Doeon Kim, Byung Joo Kim, Tae Hwan Noh and Ok-Sang Jung\*

The reaction of  $\text{CuX}_2$  ( $\text{X}^- = \text{ClO}_4^-$  and  $\text{BF}_4^-$ ) with a new 1,3,5-tris(isonicotinoyloxymethyl)benzene (L) ligand gives rise to 3D coordination networks,  $[\text{Cu}_3\text{L}_4(\text{CH}_3\text{CN})_6](\text{X})_6$ , with a new topology of the Schläfli point symbol  $\{4\cdot 8^2\}_4\{4^2\cdot 8^2\cdot 10^2\}_2\{8^4\cdot 12^2\}$ .  $[\text{Cu}_3\text{L}_4(\text{CH}_3\text{CN})_6](\text{ClO}_4)_6$  and  $[\text{Cu}_3\text{L}_4(\text{CH}_3\text{CN})_6](\text{BF}_4)_6$  networks have useful oval-shaped pores of  $11.2 \times 11.2 \times 24.8 \text{ \AA}^3$  and  $11.1 \times 11.1 \times 24.4 \text{ \AA}^3$  dimensions, respectively. These porous coordination networks act as good heterogeneous catalysts, oxidizing the catechols in the order 3,5-di-*tert*-butylcatechol (3,5-DBuCat) > 4-*tert*-butylcatechol (4-BuCat) > 4-chlorocatechol (4-ClCat). The catalytic effect of  $[\text{Cu}_3\text{L}_4(\text{CH}_3\text{CN})_6](\text{BF}_4)_6$  is slightly higher than that of  $[\text{Cu}_3\text{L}_4(\text{CH}_3\text{CN})_6](\text{ClO}_4)_6$ . The pores of the 3D networks reversibly adsorb the solvents in the order chloroform > tetrahydrofuran > acetone.

Received 14th January 2015,  
Accepted 16th February 2015

DOI: 10.1039/c5ce00087d

www.rsc.org/crystengcomm

## Introduction

One issue in the field of coordination networks is the design and construction of a new porous topology, preferably with task-specific functions<sup>1,2</sup> such as gas storage, adsorption, sensing, separation, catalysis, nonlinear optics, biomedical imaging, and drug delivery.<sup>3–10</sup> For the purposes of practical applications such as these, rational construction of unusual topological coordination polymers with desirable pores *via* manipulation of interchangeable components has been attempted. Porous coordination networks have been synthesized by suitable combination of the coordination geometry of metal ions, bonding mode and flexibility of multidentate donors, counteranions, metal-to-ligand ratio, temperature, and reaction solvents, while often versatile molecular skeletons are serendipitously constructed owing to the unexpected emergence of weak interactions such as van der Waals forces,

M–M bonds, electrostatic interactions, hydrogen bonds, and  $\pi\cdots\pi$  interactions.<sup>11–14</sup> Recently, with some of the tridentate pyridyl donor ligands, exciting molecular structures, including a variety of coordination modes, have been produced. These successes are owed to tridentate ligands' flexibility in potential bridging capacity, flexible bite angles, and conformational non-rigidity.<sup>15–22</sup> However, production of new topological skeletons *via* the reaction of simple metal ions with the  $C_3$ -symmetric tridentate ligand has proved challenging. In this context, we report the synthesis of new topological 3D copper(II) coordination networks from the reaction of  $\text{CuX}_2$  ( $\text{X}^- = \text{ClO}_4^-$  and  $\text{BF}_4^-$ ) with a new  $C_3$ -symmetric tectonic ligand, 1,3,5-tris(isonicotinoyloxymethyl)benzene (L). We additionally report the achievement of significant heterogeneous catalytic effects on catechol oxidation and molecular adsorption *via* porous structures as well as surface properties. Some copper(II) complexes are known to play important roles in oxidation catalysis chemistry, the Irving–Williams order of divalent metal ions, coordination geometry, biological functionalities, and Jahn–Teller distortion.<sup>23</sup> Notably, some copper(II) complexes containing nitrogen-donor ligands have been developed as alcohol-oxidation catalysts.<sup>24–26</sup>

Department of Chemistry, Pusan National University, Pusan 609-735, Republic of Korea. E-mail: oksjung@pusan.ac.kr; Fax: +82 51 516 7421; Tel: +82 51 510 2591

† Electronic supplementary information (ESI) available: X-ray crystal structures of L,  $[\text{Cu}_3\text{L}_4(\text{CH}_3\text{CN})_6](\text{ClO}_4)_6\cdot 19\text{H}_2\text{O}\cdot 6\text{CH}_3\text{CN}$ , and  $[\text{Cu}_3\text{L}_4(\text{CH}_3\text{CN})_6](\text{BF}_4)_6\cdot 16\text{H}_2\text{O}\cdot 5\text{CH}_3\text{CN}$ , schematic representation showing the linkage of the subunits, UV/vis spectra and the plot showing the oxidative catalytic yields of catechols using  $[\text{Cu}_3\text{L}_4(\text{CH}_3\text{CN})_6](\text{ClO}_4)_6\cdot 19\text{H}_2\text{O}\cdot 6\text{CH}_3\text{CN}$ , a mixture of  $\text{Cu}(\text{ClO}_4)_2$  and L, and only  $\text{Cu}(\text{ClO}_4)_2$  as catalysts, the plot showing the catalytic oxidation yield of catechols using the copper(II) complexes in a 2 : 1 [catalyst] : [catechol] ratio, UV/vis spectra showing the oxidation of 3,5-DBuCat using  $\text{CuCl}_2$  and  $\text{CuO}$ , IR spectra of  $[\text{Cu}_3\text{L}_4(\text{CH}_3\text{CN})_6](\text{ClO}_4)_6\cdot 19\text{H}_2\text{O}\cdot 6\text{CH}_3\text{CN}$  before and after catechol oxidation catalysis of 3,5-DBuCat, TGA/DSC curves of the copper(II) complexes, <sup>1</sup>H NMR spectra of the acetonitrile-desolvated species and solvent-reincorporated samples. CCDC 1043333, 1043334, and 1043335 for L,  $[\text{Cu}_3\text{L}_4(\text{CH}_3\text{CN})_6](\text{ClO}_4)_6\cdot 19\text{H}_2\text{O}\cdot 6\text{CH}_3\text{CN}$ , and  $[\text{Cu}_3\text{L}_4(\text{CH}_3\text{CN})_6](\text{BF}_4)_6\cdot 16\text{H}_2\text{O}\cdot 5\text{CH}_3\text{CN}$ , respectively. For ESI and crystallographic data in CIF or other electronic format see DOI: 10.1039/c5ce00087d

## Experimental

### Materials and measurements

All chemicals including copper(II) perchlorate and copper(II) tetrafluoroborate were purchased from Aldrich, and were used without further purification. Elemental microanalyses (C, H, N) were performed on crystalline samples at Pusan Center, KBSI, using a Vario-EL III. Thermal analyses were carried out under a dinitrogen atmosphere at a scan rate of

10 °C min<sup>-1</sup> using a Labsys TG-DSC 1600. Infrared spectra were obtained on a Nicolet 380 FT-IR spectrophotometer with samples prepared as KBr pellets or Nujol. <sup>1</sup>H (300 MHz) and <sup>13</sup>C (75 MHz) NMR spectra were recorded on a Varian Mercury Plus 300. The absorption spectra were recorded on a UV-vis spectrophotometer S-3150. Inductively coupled plasma atomic emission spectroscopy (ICP-AES) was performed by using a JY HORIVA spectrometer (ACTIVA) at Pusan Center, KBSI.

### Synthesis of 1,3,5-tris(isonicotinoyloxymethyl)benzene (L)

A chloroform solution of the mixture of triethylamine (5.1 mL, 35 mmol) and pyridine (0.2 mL, 2.5 mmol) was slowly added into a stirred mixture of isonicotinoyl chloride hydrochloride (2.93 g, 16.5 mmol) and 1,3,5-benzenetrimethanol (0.84 g, 5.0 mmol) in chloroform (180 mL) at 60 °C. The reaction mixture was refluxed for 12 h. The resulting solution was washed with water several times. The chloroform layer was dried over anhydrous magnesium sulfate and filtered. Evaporation of chloroform gave a white solid product in 91% yield (2.20 g). The white crude product was recrystallized from a mixture of acetone and water, and was obtained as a dihydrate crystalline product suitable for single crystal X-ray diffraction measurement. Mp 73 °C. Found: C, 62.49; H, 4.84; N, 8.11. Calc. for C<sub>27</sub>H<sub>21</sub>N<sub>3</sub>O<sub>6</sub>·2H<sub>2</sub>O: C, 62.42; H, 4.85; N, 8.09%. IR (KBr pellet, cm<sup>-1</sup>): 3430 (br), 1724 (s), 1612 (w), 1596 (w), 1562 (w), 1450 (w), 1407 (m), 1369 (w), 1326 (m), 1278 (s), 1216 (s), 1168 (w), 1126 (m), 1116 (m), 1064 (w), 993 (w), 871 (w), 850 (w), 755 (m), 725 (w), 705 (m), 682 (w), 667 (w). δ<sub>H</sub> (300 MHz, CDCl<sub>3</sub>, ppm): 8.79 (d, *J* = 4.5 Hz, 6H), 7.86 (d, *J* = 4.5 Hz, 6H), 7.53 (s, 3H), 5.44 (s, 6H). δ<sub>C</sub> NMR (75 MHz, CDCl<sub>3</sub>, ppm): 164.63, 150.43, 136.79, 136.43, 128.06, 122.67, 66.58.

### Synthesis of [Cu<sub>3</sub>L<sub>4</sub>(CH<sub>3</sub>CN)<sub>6</sub>](ClO<sub>4</sub>)<sub>6</sub>·19H<sub>2</sub>O·6CH<sub>3</sub>CN

An acetonitrile solution (12 mL) of Cu(ClO<sub>4</sub>)<sub>2</sub>·6H<sub>2</sub>O (22 mg, 0.06 mmol) was slowly diffused into a dichloromethane solution (8 mL) of L (39 mg, 0.08 mmol). Blue crystals of [Cu<sub>3</sub>L<sub>4</sub>(CH<sub>3</sub>CN)<sub>6</sub>](ClO<sub>4</sub>)<sub>6</sub>·19H<sub>2</sub>O·6CH<sub>3</sub>CN formed at the interface and were obtained in 7 days in 81% yield (57 mg). Mp 237 °C (dec.). Found: C, 44.10; H, 4.20; N, 9.38. Calc. for C<sub>132</sub>H<sub>158</sub>N<sub>24</sub>O<sub>67</sub>Cl<sub>6</sub>Cu<sub>3</sub>: C, 44.58; H, 4.48; N, 9.45%. IR (KBr pellet, cm<sup>-1</sup>): 3552 (br), 1731 (s), 1619 (w), 1564 (w), 1504 (w), 1454 (w), 1423 (m), 1373 (w), 1330 (w), 1282 (s), 1230 (w), 1122 (s), 1087 (s, ClO<sub>4</sub><sup>-</sup>), 1060 (m), 862 (w), 763 (w), 698 (w), 622 (w).

### Synthesis of [Cu<sub>3</sub>L<sub>4</sub>(CH<sub>3</sub>CN)<sub>6</sub>](BF<sub>4</sub>)<sub>6</sub>·16H<sub>2</sub>O·5CH<sub>3</sub>CN

An acetonitrile solution (12 mL) of Cu(BF<sub>4</sub>)<sub>2</sub>·*n*H<sub>2</sub>O (14 mg, 0.06 mmol) was slowly diffused into a dichloromethane solution (8 mL) of L (39 mg, 0.08 mmol). Blue crystals of [Cu<sub>3</sub>L<sub>4</sub>(CH<sub>3</sub>CN)<sub>6</sub>](BF<sub>4</sub>)<sub>6</sub>·16H<sub>2</sub>O·5CH<sub>3</sub>CN formed at the interface and were obtained in 7 days in 76% yield (51 mg). Mp 227 °C (dec.). Found: C, 45.90; H, 4.40; N, 9.40. Calc. for C<sub>130</sub>H<sub>149</sub>N<sub>23</sub>O<sub>40</sub>B<sub>6</sub>F<sub>24</sub>Cu<sub>3</sub>: C, 46.12; H, 4.44; N, 9.52%. IR (KBr

pellet, cm<sup>-1</sup>): 3585 (br), 1731 (s), 1619 (w), 1564 (w), 1504 (w), 1452 (w), 1423 (m), 1375 (w), 1330 (m), 1282(s), 1230 (w), 1124 (s), 1083 (s), 1060 (s), 1031 (s, BF<sub>4</sub><sup>-</sup>), 858 (m), 763 (w), 700 (w), 520 (w).

### Catalysis

3,5-Di-*tert*-butylcatechol (3,5-DBuCat), 4-*tert*-butylcatechol (4-BuCat), and 4-chlorocatechol (4-ClCat) were employed as oxidation catalysis substrates. Catalysis using the present products was carried out relative to the simple salts, CuX<sub>2</sub> (X<sup>-</sup> = Cl<sup>-</sup>, ClO<sub>4</sub><sup>-</sup>, BF<sub>4</sub><sup>-</sup>) and CuO:<sup>27</sup> each catalyst was treated with the respective substrate in a 1:1 mole ratio in 20 mL of chloroform at 40 °C under aerobic conditions. The catalysis was monitored with reference to the increase in absorbance at 404, 388, and 396 nm for each oxidized species, 3,5-DBuBQ, 4-BuBQ, and 4-ClBQ (BQ = benzoquinone), respectively, as a function of time.<sup>28</sup>

### Crystal structure determination

All of the X-ray data were collected on a Bruker SMART automatic diffractometer with graphite-monochromated Mo Kα radiation (λ = 0.71073 Å) and a CCD detector at -25 °C. Thirty-six frames of two-dimensional diffraction images were collected and processed to obtain the cell parameters and orientation matrix. The data were corrected for Lorentz and polarization effects. Absorption effects were corrected by the multi-scan method (SADABS).<sup>29</sup> The structures were solved by the direct method (SHELXS 97) and refined by full-matrix least squares techniques (SHELXL 97).<sup>30</sup> The non-hydrogen atoms were refined anisotropically, and the hydrogen atoms were placed in calculated positions and refined using a riding model. Structure refinement of all of the compounds for the disordered electron density, using the SQUEEZE routine<sup>31</sup> in PLATON, led to better refinement (see the ESI† for details). The final formulae [Cu<sub>3</sub>L<sub>4</sub>(CH<sub>3</sub>CN)<sub>6</sub>](ClO<sub>4</sub>)<sub>6</sub>·19H<sub>2</sub>O·6CH<sub>3</sub>CN and [Cu<sub>3</sub>L<sub>4</sub>(CH<sub>3</sub>CN)<sub>6</sub>](BF<sub>4</sub>)<sub>6</sub>·16H<sub>2</sub>O·5CH<sub>3</sub>CN were determined by combined elemental and thermal analyses and <sup>1</sup>H NMR spectroscopic measurement. The crystal parameters and procedural information corresponding to the data collection and structure refinement are listed in Table 1.

## Results and discussion

### Synthetic aspects

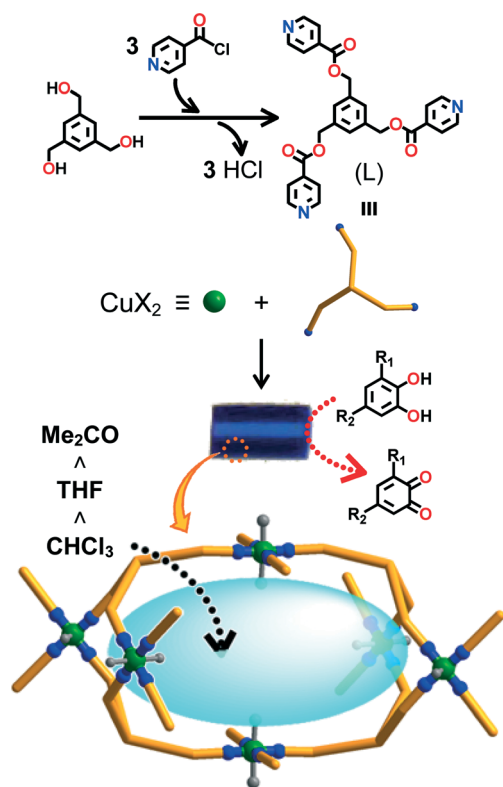
The new ligand, 1,3,5-tris(isonicotinoyloxymethyl)benzene (L), was synthesized in a high yield by the reaction of 1,3,5-benzene-trimethanol with isonicotinoyl chloride in chloroform in the presence of an excess amount of triethylamine and pyridine. Recrystallization of the crude product from a mixture of acetone and water afforded colorless single crystals suitable for X-ray diffraction measurement. Self-assembly of acetonitrile solution of CuX<sub>2</sub> (X<sup>-</sup> = ClO<sub>4</sub><sup>-</sup> and BF<sub>4</sub><sup>-</sup>) with dichloromethane solution of L produced blue parallel-pipe-shaped single crystals consisting of 3D coordination polymers and [Cu<sub>3</sub>L<sub>4</sub>(CH<sub>3</sub>CN)<sub>6</sub>](X)<sub>6</sub> composition in high yields, as

**Table 1** Crystal refinement parameters for L,  $[\text{Cu}_3\text{L}_4(\text{CH}_3\text{CN})_6](\text{ClO}_4)_6 \cdot 19\text{H}_2\text{O} \cdot 6\text{CH}_3\text{CN}$ , and  $[\text{Cu}_3\text{L}_4(\text{CH}_3\text{CN})_6](\text{BF}_4)_6 \cdot 16\text{H}_2\text{O} \cdot 5\text{CH}_3\text{CN}$ 

	L·2H <sub>2</sub> O	$[\text{Cu}_3\text{L}_4(\text{CH}_3\text{CN})_6](\text{ClO}_4)_6 \cdot 19\text{H}_2\text{O} \cdot 6\text{CH}_3\text{CN}$	$[\text{Cu}_3\text{L}_4(\text{CH}_3\text{CN})_6](\text{BF}_4)_6 \cdot 16\text{H}_2\text{O} \cdot 5\text{CH}_3\text{CN}$
Formula*	C <sub>27</sub> H <sub>25</sub> N <sub>3</sub> O <sub>8</sub>	C <sub>120</sub> H <sub>102</sub> N <sub>18</sub> O <sub>48</sub> Cl <sub>6</sub> Cu <sub>3</sub>	C <sub>120</sub> H <sub>102</sub> N <sub>18</sub> O <sub>24</sub> Cu <sub>3</sub>
M <sub>w</sub> *	519.50	2967.52	2370.82
Crystal system	Triclinic	Monoclinic	Orthorhombic
Space group	<i>P</i> $\bar{1}$	<i>C</i> 2/ <i>c</i>	<i>Ibam</i>
<i>a</i> (Å)	7.4117(4)	41.190(1)	20.6958(5)
<i>b</i> (Å)	12.1658(6)	20.6334(4)	27.2441(9)
<i>c</i> (Å)	14.2115(7)	27.0979(8)	31.2425(7)
$\alpha$ (°)	85.918(3)	90	90
$\beta$ (°)	77.087(3)	129.772(3)	90
$\gamma$ (°)	77.944(3)	90	90
<i>V</i> (Å <sup>3</sup> )	1221.1(1)	17700.8(8)	17615.7(8)
$\sigma$ (Mg m <sup>-3</sup> )*	1.413	1.114	0.894
<i>Z</i>	2	4	4
$\mu$ (mm <sup>-1</sup> )	0.106	0.519	0.411
<i>R</i> <sub>int</sub>	0.0384	0.0756	0.1735
Data/parameters	5054/343	17 337/879	8843/461
Completeness (%)	99.9 ( $\theta = 26.50^\circ$ )	99.6 ( $\theta = 26.00^\circ$ )	100.0 ( $\theta = 26.00^\circ$ )
GoF on <i>F</i> <sup>2</sup>	1.024	0.951	0.851
<i>R</i> <sub>1</sub> <sup>a</sup>	0.0454	0.0942	0.0864
w <i>R</i> <sub>2</sub> <sup>b</sup>	0.1167	0.2965	0.2720

<sup>a</sup>  $R_1 = \sum ||F_o| - |F_c|| / \sum |F_o|$ . <sup>b</sup>  $wR_2 = (\sum [w(F_o^2 - F_c^2)^2] / \sum [w(F_o^2)^2])^{1/2}$ . \*The solvent molecules (in both cases) and anions (in the case of  $[\text{Cu}_3(\text{L})_4(\text{CH}_3\text{CN})_6](\text{BF}_4)_6 \cdot 16\text{H}_2\text{O} \cdot 5\text{CH}_3\text{CN}$ ) of the copper(II) complexes are missing from the formula. Due to extensive disorder, they could not be located.

shown in Scheme 1. The copper(II) networks' formation of 3 : 4 composition products was attributed to the intrinsic properties of the *C*<sub>3</sub>-symmetric tectonic L and copper(II) ions. That



**Scheme 1** Procedure for synthesis of 3D copper(II) networks,  $[\text{Cu}_3\text{L}_4(\text{CH}_3\text{CN})_6](\text{X})_6$  ( $\text{X}^- = \text{ClO}_4^-$  and  $\text{BF}_4^-$ ). The gray balls represent the coordinating acetonitrile molecules.

is, the assembly reaction was initially conducted in a 1 : 1 copper(II) ion : L mole ratio, but the product formation was not significantly affected by the change in the reactants' mole ratio and concentration, indicating that the 3 : 4 composition products were thermodynamically stable. Crystalline solid products (except for solvate molecules, which evaporate on crystal surfaces) are stable under aerobic conditions, and are insoluble in water and common organic solvents such as acetone, benzene, chloroform, ethyl acetate, and tetrahydrofuran, but are dissociated in strong polar solvents such as acetonitrile, dimethyl sulfoxide, and *N,N*-dimethylformamide. Thus, it was found that the combined effects of the stable tridentate ligand and the appropriate copper(II) geometry, along with the coordinating capacity of solvate acetonitrile, might be a significant driving force behind the formation of the unusual 3D network species. The compositions and structures were confirmed by elemental analyses, IR, thermal analysis, and X-ray single crystallography. The characteristic strong IR bands at 1087 and 1031  $\text{cm}^{-1}$  were found to correspond to  $\text{ClO}_4^-$  and  $\text{BF}_4^-$ , respectively.

### Crystal structures

The new L was fully characterized by X-ray single crystallography. The crystal structure of L·2H<sub>2</sub>O is depicted in Fig. S1 (ESI†). The dihedral angles between the central benzyl plane and each pyridyl moiety were determined to be 11.80(6), 18.99(7), and 27.70(4)°. There are intermolecular  $\pi \cdots \pi$  interactions between the adjacent central benzyl groups (3.58(2) Å and 0.00(5)° for the distance and dihedral angle, respectively) and the pyridyl groups (3.58(2) Å and 0.00(8)° for the distance and dihedral angle, respectively). X-ray

crystallographic characterization revealed that the skeletons of  $[\text{Cu}_3\text{L}_4(\text{CH}_3\text{CN})_6](\text{ClO}_4)_6 \cdot 19\text{H}_2\text{O} \cdot 6\text{CH}_3\text{CN}$  and  $[\text{Cu}_3\text{L}_4(\text{CH}_3\text{CN})_6](\text{BF}_4)_6 \cdot 16\text{H}_2\text{O} \cdot 5\text{CH}_3\text{CN}$  are, as depicted in Fig. 1, 3D coordination frameworks. Their relevant bond lengths and angles are listed in Table 2. For  $[\text{Cu}_3\text{L}_4(\text{CH}_3\text{CN})_6](\text{ClO}_4)_6 \cdot 19\text{H}_2\text{O} \cdot 6\text{CH}_3\text{CN}$ , there are two crystallographically independent copper(II) ions, two L, three coordinating  $\text{CH}_3\text{CN}$  molecules, and three perchlorate counteranions in an asymmetric unit, as indicated in Fig. S2 (ESI<sup>†</sup>). Each L connects three copper(II) ions to produce the 3D network. The coordinating environment of the copper(II) ions is a typical octahedral geometry with four N-donors from four L ( $\text{Cu}-\text{N} = 2.02(3)–2.03(3)$  Å) in a basal plane and with two N-donors from two coordinating  $\text{CH}_3\text{CN}$  molecules ( $\text{Cu}-\text{N} = 2.47(4)–2.61(4)$  Å) in the axial position. The axial  $\text{Cu}-\text{N}$  bond elongation seems to come from the typical Jahn–Teller distortion of a  $d^9$ -Cu(II) system.<sup>32</sup> In order to simplify the structural representation of the present copper(II) complexes, a topological analysis was performed. As shown in Fig. 1, L can be defined as a 3-connected node, and two copper(II) centers act as 4-connected nodes, resulting in a 3D coordination network of a new trinodal 3,4,4-connected net topology with the Schläfli point symbol  $\{4 \cdot 8^2\}_4\{4^2 \cdot 8^2 \cdot 10^2\}_2\{8^4 \cdot 12^2\}$ .<sup>33</sup> This 3D network basically consists of oval-shaped cages, in which two Cu(1) are positioned on the top and bottom facets, and four Cu(2) are set in the apex (Fig. S1 and S2, ESI<sup>†</sup>). The intracage  $\text{Cu}(1) \cdots \text{Cu}(1)$  distances are 15.8336(7) Å and 15.6213(4) Å for  $[\text{Cu}_3\text{L}_4(\text{CH}_3\text{CN})_6](\text{ClO}_4)_6 \cdot 19\text{H}_2\text{O} \cdot 6\text{CH}_3\text{CN}$  and  $[\text{Cu}_3\text{L}_4(\text{CH}_3\text{CN})_6](\text{BF}_4)_6 \cdot 16\text{H}_2\text{O} \cdot 5\text{CH}_3\text{CN}$ , respectively, and their

lateral  $\text{Cu}(2) \cdots \text{Cu}(2)$  distances are 12.783(6); 24.342(7) Å and 12.788(2); 24.288(2) Å, respectively. As shown in Fig. S3 (ESI<sup>†</sup>), the unit cages are connected through Cu(2) in the crystallographic  $bc$ -direction, and are linked through Cu(1) to form 1D linked cages running perpendicular to the  $bc$ -plane. The pore dimensions were determined to be  $11.2 \times 11.2 \times 24.8$  Å<sup>3</sup> and  $11.1 \times 11.1 \times 24.4$  Å<sup>3</sup> for  $[\text{Cu}_3\text{L}_4(\text{CH}_3\text{CN})_6](\text{ClO}_4)_6$  and  $[\text{Cu}_3\text{L}_4(\text{CH}_3\text{CN})_6](\text{BF}_4)_6$ , respectively. The porous volume is filled with solvent molecules and counteranions for the cationic skeleton (Fig. 2).

### Catalytic oxidation of catechols

Both of the 3D copper(II) networks were subjected to catecholase-mimetics to determine their catalytic activity in the oxidation of catechols to the corresponding *o*-benzoquinones. In order to elucidate the substituent effects of substrates on the catalytic activity, 3,5-di-*tert*-butylcatechol (3,5-DBuCat), 4-*tert*-butylcatechol (4-BuCat), and 4-chlorocatechol (4-ClCat) have been employed as catalytic reaction substrates, because their low potentials allow for their smooth oxidation without side reactions,<sup>34</sup> and also because their oxidized *o*-benzoquinone species have been very useful ligands for non-innocent intramolecular electron transfer molecular systems<sup>35,36</sup> that exhibit a  $\lambda_{\text{max}}$  absorption band around 390–400 nm.<sup>28</sup> Thus, in the present study, their catalytic activities, including reaction rates, listed in Table 3, were easily determined according to the increase in absorbance of the oxidized *o*-benzoquinone species as a function of time. To this end, each catalyst was treated with the respective catechol substrate in a 1:1 molar ratio in 20 mL of chloroform at 40 °C under aerobic conditions. For  $[\text{Cu}_3\text{L}_4(\text{CH}_3\text{CN})_6](\text{ClO}_4)_6 \cdot 19\text{H}_2\text{O} \cdot 6\text{CH}_3\text{CN}$ , the oxidations of 3,5-DBuCat, 4-BuCat, and 4-ClCat were completed within 8, 12, and 15 h, respectively (Fig. S4, ESI<sup>†</sup>). The respective turnover frequencies (TOFs) for 3,5-DBuCat, 4-BuCat, and 4-ClCat were determined to be 0.125, 0.083, and 0.067 h<sup>-1</sup>. That is, the catalytic rates were in the order 3,5-DBuCat > 4-BuCat > 4-ClCat, which indicated that the reaction rate was dependent on the electron-donating ability of the catechol substituents.<sup>37,38</sup> By comparison, the catalytic reactions using  $[\text{Cu}_3\text{L}_4(\text{CH}_3\text{CN})_6](\text{BF}_4)_6 \cdot 16\text{H}_2\text{O} \cdot 5\text{CH}_3\text{CN}$  were completed within 4, 6, and 12 h, respectively (Fig. 3 and S5, ESI<sup>†</sup>), and the corresponding TOFs were 0.25, 0.167, and 0.083 h<sup>-1</sup>, respectively, indicating that  $[\text{Cu}_3\text{L}_4(\text{CH}_3\text{CN})_6](\text{BF}_4)_6 \cdot 16\text{H}_2\text{O} \cdot 5\text{CH}_3\text{CN}$  is more effective than  $[\text{Cu}_3\text{L}_4(\text{CH}_3\text{CN})_6](\text{ClO}_4)_6 \cdot 19\text{H}_2\text{O} \cdot 6\text{CH}_3\text{CN}$ . Such a fact can be explained by the tetrafluoroborate anion's superior lipophilicity relative to the perchlorate anion in chloroform. That is, it helps with the substrate diffusion into the 3D porous network of the crystal surface in chloroform media. When the amount of catalyst was increased twice, the catalytic rates increased significantly (Fig. S6, ESI<sup>†</sup>). Additionally, interesting results were obtained in control experiments by employing the simple mixtures of  $\text{CuX}_2$  ( $\text{X}^- = \text{ClO}_4^-$  and  $\text{BF}_4^-$ ) and L in a 3:4 mole ratio. As depicted in Fig. 3 and S3 (ESI<sup>†</sup>), the catalytic oxidations using the simple mixtures

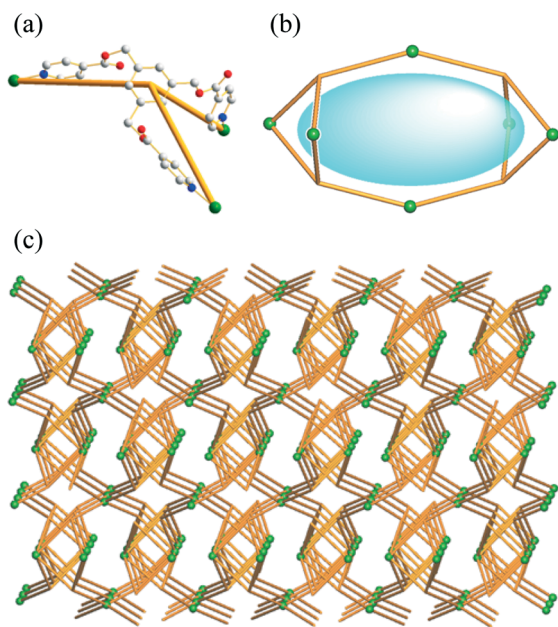


**Fig. 1** Topological representation of  $[\text{Cu}_3\text{L}_4(\text{CH}_3\text{CN})_6](\text{ClO}_4)_6 \cdot 19\text{H}_2\text{O} \cdot 6\text{CH}_3\text{CN}$ : (a) ball-and-stick diagram of 3-connected L with schematic connectivity to three neighboring copper(II) ions, (b) schematic drawing of the subunit, and (c) 3-D coordinating framework with a new Schläfli point symbol of  $\{4 \cdot 8^2\}_4\{4^2 \cdot 8^2 \cdot 10^2\}_2\{8^4 \cdot 12^2\}$ .

**Table 2** Selected bond lengths (Å) and angles (°) for  $[\text{Cu}_3\text{L}_4(\text{CH}_3\text{CN})_6](\text{ClO}_4)_6 \cdot 19\text{H}_2\text{O} \cdot 6\text{CH}_3\text{CN}$  and  $[\text{Cu}_3\text{L}_4(\text{CH}_3\text{CN})_6](\text{BF}_4)_6 \cdot 16\text{H}_2\text{O} \cdot 5\text{CH}_3\text{CN}^a$ 

$[\text{Cu}_3\text{L}_4(\text{CH}_3\text{CN})_6](\text{ClO}_4)_6 \cdot 19\text{H}_2\text{O} \cdot 6\text{CH}_3\text{CN}$		$[\text{Cu}_3\text{L}_4(\text{CH}_3\text{CN})_6](\text{BF}_4)_6 \cdot 16\text{H}_2\text{O} \cdot 5\text{CH}_3\text{CN}$	
Cu(1)–N(1)	2.03(2)	Cu(1)–N(2)	2.054(4)
Cu(1)–N(4)	2.03(2)	Cu(1)–N(6)	2.354(7)
Cu(1)–N(7)	2.50(4)	Cu(2)–N(1)	2.035(6)
Cu(2)–N(2) <sup>#1</sup>	2.02(3)	Cu(2)–N(3) <sup>#6</sup>	2.000(6)
Cu(2)–N(3) <sup>#2</sup>	2.02(3)	Cu(2)–N(4)	2.341(7)
Cu(2)–N(5) <sup>#3</sup>	2.03(3)	Cu(2)–N(5)	2.374(8)
Cu(2)–N(6)	2.02(3)		
Cu(2)–N(8)	2.61(4)		
Cu(2)–N(9)	2.47(4)		
N(1)–Cu(1)–N(4)	175.5(1)	N(2)–Cu(1)–N(2) <sup>#7</sup>	91.4(3)
N(1)–Cu(1)–N(1) <sup>#4</sup>	91.7(9)	N(2)–Cu(1)–N(2) <sup>#8</sup>	88.8(3)
N(1)–Cu(1)–N(7)	94.6(1)	N(2)–Cu(1)–N(2) <sup>#9</sup>	175.1(3)
N(7)–Cu(1)–N(7) <sup>#5</sup>	176.1(1)	N(2) <sup>#7</sup> –Cu(1)–N(2) <sup>#8</sup>	175.1(1)
N(2) <sup>#1</sup> –Cu(1)–N(6)	91.1(1)	N(6)–Cu(1)–N(6) <sup>#8</sup>	180.0
N(3) <sup>#2</sup> –Cu(1)–N(6)	89.0(1)	N(1)–Cu(2)–N(1) <sup>#10</sup>	90.4(3)
N(5) <sup>#3</sup> –Cu(1)–N(6)	178.7(1)	N(1)–Cu(2)–N(3) <sup>#6</sup>	179.3(3)
N(2) <sup>#1</sup> –Cu(1)–N(3) <sup>#2</sup>	175.5(1)	N(1) <sup>#10</sup> –Cu(2)–N(3) <sup>#11</sup>	179.3(3)
N(8)–Cu(2)–N(9)	178.2(1)	N(4)–Cu(2)–N(5)	179.3(4)

<sup>a</sup> Symmetry codes: #1  $-x + 1/2, -y + 3/2, -z + 1$ , #2  $x, -y + 1, z - 1/2$ , #3  $-x + 1/2, y - 1/2, -z + 1/2$ , #4  $-x + 1, y, -z + 3/2$ , #5  $-x + 1, y, -z + 3/2$ , #6  $x - 1/2, -y + 1/2, -z$ , #7  $-x - 2, y, -z + 1/2$ , #8  $x, -y, -z + 1/2$ , #9  $-x - 2, -y, z$ , #10  $x, y, -z$ , #11  $x - 1/2, -y + 1/2, z$ .

were negligible (less than 10%) until 24 h, but were significant after 24 h. This result indicated that the catalytic reaction proceeded after the formation of the copper(II) frameworks. When simple salts,  $\text{CuX}_2$  ( $\text{X}^- = \text{Cl}^-, \text{ClO}_4^-, \text{and BF}_4^-$ ), were used as catalysts (Fig. S7, ESI<sup>†</sup>), the catalytic effects (3–12%) were of course very low compared with those of the present 3D network catalytic systems. Such a fact suggests

that the structures including the surface properties of the present 3D porous materials play an important role in the catalysis. Crucially, the cages and their windows are sufficiently large to allow the catechol substrates' access. The catalytic mechanism of the present copper(II) systems appears to be the same as that of other copper(II)-based complexes, which involves complexation of the catechol to a vacant site on the copper(II) center, oxidation of the catechol by molecular oxygen, and subsequent release of the product.<sup>21,39,40</sup> These porous catalytic systems are not much more effective than that of dinuclear copper(II) complexes for mimicking naturally occurring enzymes through four-electron reduction of molecular oxygen to water.<sup>41–43</sup> Since the two 3D copper(II) networks were not dissociated in chloroform during catalysis, the recyclability of the heterogeneous catalytic systems was tested. An 80 mg sample of each 3D copper(II) network was employed as a catalyst, and the catalytic oxidation of 3,5-DBuCat (5 mg) in 20 mL of chloroform was carried out for 3 h at 40 °C. Upon completion of the oxidation, the

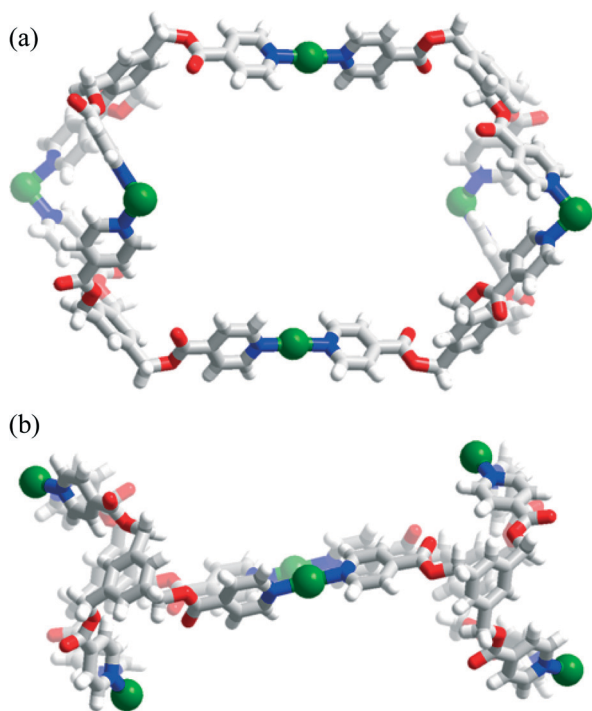


**Fig. 2** Side (a) and top (b) views showing the unit cage of  $[\text{Cu}_3\text{L}_4(\text{CH}_3\text{CN})_6](\text{ClO}_4)_6 \cdot 19\text{H}_2\text{O} \cdot 6\text{CH}_3\text{CN}$ . The counteranions and coordinating acetonitrile molecules were omitted for clarity.

**Table 3** Catalytic yields for catechol oxidation<sup>c</sup>

Entry	Catalyst	Catechols	Yield (%)
1	<sup>a</sup>	3,5-DBuCat	98
2	<sup>a</sup>	4-BuCat	93
3	<sup>a</sup>	4-CuCat	41
4	<sup>b</sup>	3,5-DBuCat	100
5	<sup>b</sup>	4-BuCat	100
6	<sup>b</sup>	4-CuCat	89
7	$\text{Cu}(\text{ClO}_4)_2$	3,5-DBuCat	9
8	$\text{Cu}(\text{BF}_4)_2$	3,5-DBuCat	7
9	$\text{CuO}$	3,5-DBuCat	3

<sup>a</sup>  $[\text{Cu}_3\text{L}_4(\text{CH}_3\text{CN})_6](\text{ClO}_4)_6 \cdot 19\text{H}_2\text{O} \cdot 6\text{CH}_3\text{CN}$ . <sup>b</sup>  $[\text{Cu}_3\text{L}_4(\text{CH}_3\text{CN})_6](\text{BF}_4)_6 \cdot 16\text{H}_2\text{O} \cdot 5\text{CH}_3\text{CN}$ . <sup>c</sup> The [catalyst]:[catechol] ratio was 1:1. The catalytic reaction time and temperature were 6 h and 40 °C, respectively.

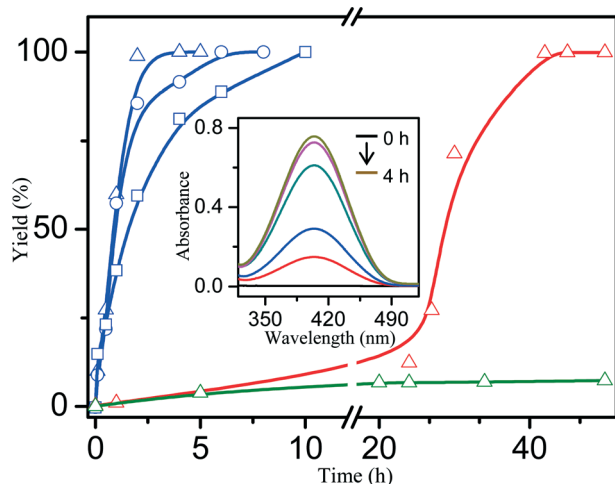


**Fig. 3** Plot showing catalytic yields of 3,5-DBuCat (triangle), 4-BuCat (circle), and 4-ClCat (squares) using  $[\text{Cu}_3\text{L}_4(\text{CH}_3\text{CN})_6](\text{BF}_4)_6 \cdot 16\text{H}_2\text{O} \cdot 5\text{CH}_3\text{CN}$  (blue lines), a mixture of  $\text{Cu}(\text{BF}_4)_2$  and L in a 3:4 ratio (red line), and only  $\text{Cu}(\text{BF}_4)_2$  (green line) as catalysts. The [catalyst]:[catechol] ratio was 1:1 in  $\text{CHCl}_3$  at 40 °C. Inset: UV/vis spectra showing the oxidation of 3,5-DBuCat to 3,5-DBuBQ using  $[\text{Cu}_3\text{L}_4(\text{CH}_3\text{CN})_6](\text{BF}_4)_6 \cdot 16\text{H}_2\text{O} \cdot 5\text{CH}_3\text{CN}$  as a heterogeneous catalyst.

catalyst was simply filtered off and reused for the next catalysis. As plotted in Fig. 4, the catalytic activity in both cases gradually declined over the course of four consecutive reactions. The heterogeneity of the catalytic reactions was evaluated by inductively coupled plasma atomic emission spectroscopy (ICP-AES) analysis of the post-catalysis supernatant. As expected, copper(II) cations were scarce in both cases (not detected for  $[\text{Cu}_3\text{L}_4(\text{CH}_3\text{CN})_6](\text{ClO}_4)_6 \cdot 19\text{H}_2\text{O} \cdot 6\text{CH}_3\text{CN}$ ; 0.01 ppm for  $[\text{Cu}_3\text{L}_4(\text{CH}_3\text{CN})_6](\text{BF}_4)_6 \cdot 16\text{H}_2\text{O} \cdot 5\text{CH}_3\text{CN}$ ), indicating that the 3D coordinating framework was robust during the catalytic reactions. Also, the IR spectra of the as-synthesized

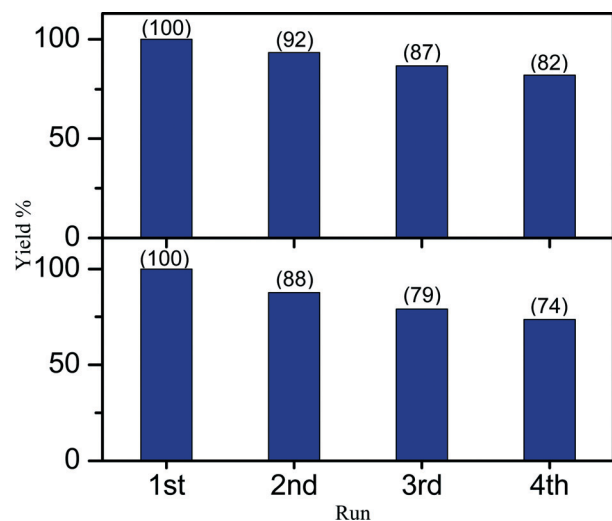


**Fig. 4** Recycling test of  $[\text{Cu}_3\text{L}_4(\text{CH}_3\text{CN})_6](\text{ClO}_4)_6 \cdot 19\text{H}_2\text{O} \cdot 6\text{CH}_3\text{CN}$  (top) and  $[\text{Cu}_3\text{L}_4(\text{CH}_3\text{CN})_6](\text{BF}_4)_6 \cdot 16\text{H}_2\text{O} \cdot 5\text{CH}_3\text{CN}$  (bottom) catalysts for oxidation of 3,5-DBuCat.

copper(II) catalysts and the four-time-recycled catalysts were shown to be identical (Fig. S8, ESI†).

### Thermal behavior and solvent adsorption

Thermogravimetric analysis (TGA) and differential scanning calorimetry (DSC) overlays of the 3D copper(II) networks demonstrated that the skeletons of  $[\text{Cu}_3\text{L}_4(\text{CH}_3\text{CN})_6](\text{ClO}_4)_6 \cdot 19\text{H}_2\text{O} \cdot 6\text{CH}_3\text{CN}$  and  $[\text{Cu}_3\text{L}_4(\text{CH}_3\text{CN})_6](\text{BF}_4)_6 \cdot 16\text{H}_2\text{O} \cdot 5\text{CH}_3\text{CN}$  had drastically collapsed at 237 and 227 °C, respectively (Fig. 5 and S9, ESI†). Prior to this thermal decomposition, both the coordinating and solvate acetonitrile molecules evaporated in the 30–95 and 30–105 °C range, respectively ( $[\text{Cu}_3\text{L}_4(\text{CH}_3\text{CN})_6](\text{ClO}_4)_6 \cdot 19\text{H}_2\text{O} \cdot 6\text{CH}_3\text{CN}$ : calcd. 13.9%, found 9.4%;  $[\text{Cu}_3\text{L}_4(\text{CH}_3\text{CN})_6](\text{BF}_4)_6 \cdot 16\text{H}_2\text{O} \cdot 5\text{CH}_3\text{CN}$ : calcd. 13.3%, found 13.0%). However, the solvate water molecules were safely nestled in the 3D framework, as confirmed by the relevant IR and  $^1\text{H}$  NMR spectra. As depicted in Fig. 5, the  $\tilde{\nu}_{\text{C}\equiv\text{N}}$  band at 2251  $\text{cm}^{-1}$  (in a Nujol mull) disappeared after the sample was evacuated at 80 °C for 1 day, whereas the  $\tilde{\nu}_{\text{OH}}$  band in the 3300–3600  $\text{cm}^{-1}$  range was retained.

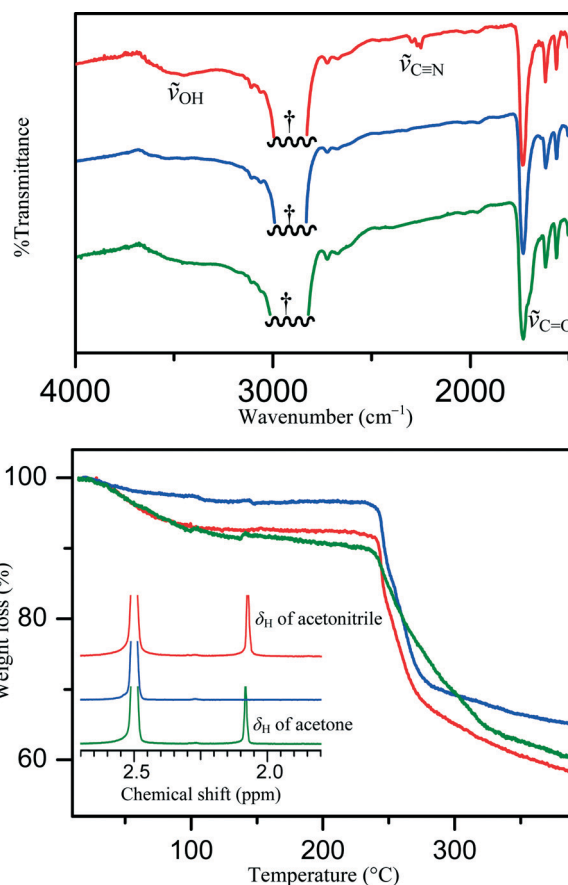


**Fig. 5** IR (Nujol mull) spectra (top), TGA curves (bottom), and partial  $^1\text{H}$  NMR ( $\text{Me}_2\text{SO}-d_6$ ) spectra (inset in bottom) of  $[\text{Cu}_3\text{L}_4(\text{CH}_3\text{CN})_6](\text{ClO}_4)_6 \cdot 19\text{H}_2\text{O} \cdot 6\text{CH}_3\text{CN}$  (red), acetonitrile-desolvated  $[\text{Cu}_3\text{L}_4](\text{ClO}_4)_6 \cdot 19\text{H}_2\text{O}$  (blue), and acetone-adsorbed  $[\text{Cu}_3\text{L}_4](\text{ClO}_4)_6 \cdot 19\text{H}_2\text{O} \cdot 7\text{Me}_2\text{CO}$  (green). The daggers denote the vibrational frequency corresponding to the  $\text{sp}^3$  hydrocarbon of Nujol.

In order to determine the adsorption ability of versatile organic solvent molecules, the acetonitrile-free species,  $[\text{Cu}_3\text{L}_4](\text{ClO}_4)_6 \cdot 19\text{H}_2\text{O}$ , was immersed in chloroform, tetrahydrofuran (THF), and acetone. Thus, the incorporated solvent molecules could be checked by  $^1\text{H}$  NMR in  $\text{Me}_2\text{SO}-d_6$  even though the 3D coordination skeletons were dissociated in  $\text{Me}_2\text{SO}-d_6$ . Within 24 h, solvent adsorption was accomplished (Fig. S10, ESI<sup>†</sup>) yielding  $[\text{Cu}_3\text{L}_4](\text{ClO}_4)_6 \cdot 19\text{H}_2\text{O} \cdot 12\text{CHCl}_3$ ,  $[\text{Cu}_3\text{L}_4](\text{ClO}_4)_6 \cdot 19\text{H}_2\text{O} \cdot 13\text{THF}$ , and  $[\text{Cu}_3\text{L}_4](\text{ClO}_4)_6 \cdot 19\text{H}_2\text{O} \cdot 7\text{Me}_2\text{CO}$ , respectively. The IR spectra corresponding to the species' skeleton remained virtually unchanged, suggesting that the 3D coordination network is retained after solvent adsorption (Fig. 5). The same experiment employing the acetonitrile-free species  $[\text{Cu}_3\text{L}_4](\text{BF}_4)_6 \cdot 16\text{H}_2\text{O}$  produced  $[\text{Cu}_3\text{L}_4](\text{BF}_4)_6 \cdot 16\text{H}_2\text{O} \cdot 7\text{CHCl}_3$ ,  $[\text{Cu}_3\text{L}_4](\text{BF}_4)_6 \cdot 16\text{H}_2\text{O} \cdot 8\text{THF}$ , and  $[\text{Cu}_3\text{L}_4](\text{BF}_4)_6 \cdot 16\text{H}_2\text{O} \cdot 4\text{acetone}$ , respectively (Fig. 5 and S11, ESI<sup>†</sup>). Further, the acetonitrile-desolvated species  $[\text{Cu}_3\text{L}_4](\text{ClO}_4)_6 \cdot 19\text{H}_2\text{O}$  and  $[\text{Cu}_3\text{L}_4](\text{BF}_4)_6 \cdot 16\text{H}_2\text{O}$  were immersed in a mixture of chloroform, tetrahydrofuran, and acetone (v/v/v = 1:1:1) for 1 day, resulting in the incorporation of chloroform, tetrahydrofuran, and acetone in 5:2:1 and 3:2:1 ratios, respectively (Fig. S12, ESI<sup>†</sup>). This might be ascribed to the polarity of the solvent molecules rather than the coordinating ability or size effects.

## Conclusions

Reactions of  $\text{CuX}_2$  ( $\text{X}^- = \text{ClO}_4^-$  and  $\text{BF}_4^-$ ) with a new 1,3,5-tris(isonicotinoyloxymethyl)benzene (L) ligand give rise to unusual 3D,  $[\text{Cu}_3\text{L}_4(\text{CH}_3\text{CN})_6](\text{X})_6$  coordination networks, with a new topology of the Schläfli point symbol  $\{4 \cdot 8^2\}_4\{4^2 \cdot 8^2 \cdot 10^2\}_2\{8^4 \cdot 12^2\}$ . The 3D network basically has oval-shaped pores that are useful for heterogeneous catalysis and adsorption. The catalytic oxidation rates of the catechols to *o*-benzoquinone were in the order 3,5-DBuCat > 4-BuCat > 4-ClCat, due to the electron-donating ability of the substituents. The molecular-accessible spaces adsorbed the solvents reversibly in the order  $\text{CHCl}_3 > \text{THF} > \text{Me}_2\text{CO}$ . A further study on this series of coordination frameworks based on the *N*-donor tridentate ligand is under way, the results of which could offer a systematic strategy for the design and construction of MOFs with new topologies, not to mention potential applications in gas separation or adsorption.

## Acknowledgements

This work was supported by a grant from the National Research Foundation of Korea (NRF) funded by the Korean Government [MEST] (2013R1A2A2A07067841).

## Notes and references

- C. B. Aakeröy, N. R. Champness and C. Janiak, *CrystEngComm*, 2010, **12**, 22–43.
- C. Mellot-Draznieks, J. Dutour and G. Férey, *Angew. Chem., Int. Ed.*, 2004, **43**, 6290–6296.
- P. J. Stang and B. Olenyuk, *Acc. Chem. Res.*, 1997, **30**, 502–518.
- H. Chun, D. N. Dybtsev, H. Kim and K. Kim, *Chem. – Eur. J.*, 2005, **11**, 3521–3529.
- K. Uemura, R. Matsuda and S. Kitagawa, *J. Solid State Chem.*, 2005, **178**, 2420–2429.
- P. J. Steel, *Acc. Chem. Res.*, 2005, **38**, 243–250.
- C. J. Jones, *Chem. Soc. Rev.*, 1998, **27**, 289–299.
- M. W. Hosseini, *Acc. Chem. Res.*, 2005, **38**, 313–323.
- D. Bradshaw, J. B. Claridge, E. J. Cussen, T. J. Prior and M. J. Rosseinsky, *Acc. Chem. Res.*, 2005, **38**, 273–282.
- A. Clough, S.-T. Zheng, X. Zhao, Q. Lin, P. Feng and X. Bu, *Cryst. Growth Des.*, 2014, **14**, 897–900.
- G. R. Desiraju, in *The crystal as a supramolecular entity: perspectives in supramolecular chemistry*, John Wiley & Sons, New York, 1996, vol. 2.
- M. Du, X.-H. Bu, Z. Huang, S.-T. Chen and Y.-M. Guo, *Inorg. Chem.*, 2003, **42**, 552–559.
- M. Du, X.-H. Bu, Y.-M. Cuo, J. Ribas and C. Diaz, *Chem. Commun.*, 2002, 2550–2551.
- S. Y. Moon, E. Kim, T. H. Noh, Y.-A. Lee and O.-S. Jung, *Dalton Trans.*, 2013, **42**, 13974–13980.
- T. H. Noh, E. Heo, K. H. Park and O.-S. Jung, *J. Am. Chem. Soc.*, 2011, **133**, 1236–1239.
- M. Fujita, N. Fujita, K. Ogura and K. Yamagichi, *Nature*, 1999, **400**, 52–55.
- S. Ghosh and P. S. Mukherjee, *J. Org. Chem.*, 2006, **71**, 8412–8416.
- D. Moon, S. Kang, J. Park, K. Lee, R. P. John, H. Won, G. H. Seong, Y. S. Kim, H. Rhee and M. S. Lah, *J. Am. Chem. Soc.*, 2006, **128**, 3530–3531.
- H. Lee, T. H. Noh and O.-S. Jung, *Angew. Chem., Int. Ed.*, 2013, **52**, 11790–11795.
- H. Lee, T. H. Noh and O.-S. Jung, *CrystEngComm*, 2013, **15**, 1832–1835.
- W. Hong, H. Lee, T. H. Noh and O.-S. Jung, *Dalton Trans.*, 2013, **42**, 11092–11099.
- S. Hasegawa, S. Horike, R. Matsuda, S. Furukawa, K. Mochizuki, Y. Kinoshita and S. Kitagawa, *J. Am. Chem. Soc.*, 2007, **129**, 2607–2614.
- A. Puzari and J. B. Baruah, *J. Mol. Catal. A: Chem.*, 2002, **187**, 149–162.
- L. M. Berreau, S. Mahapatra, J. A. Halfen, R. P. Hauser, V. G. Young Jr. and W. B. Tolman, *Angew. Chem., Int. Ed.*, 1999, **38**, 207–210.
- P. Gentschev, N. Möller and B. Krebs, *Inorg. Chim. Acta*, 2000, **300–302**, 442–452.
- O. Das and T. K. Paine, *Dalton Trans.*, 2012, **41**, 11476–11481.
- A. Biswas, L. K. Das, M. G. B. Drew, C. Diaz and A. Ghosh, *Inorg. Chem.*, 2012, **51**, 10111–10121.
- N. Oishi, Y. Nishida, K. Ida and S. Kida, *Bull. Chem. Soc. Jpn.*, 1980, **53**, 2847–2850.
- G. M. Sheldrick, *SADABS, Program for empirical absorption correction of area detector data*, University of Göttingen, Germany, 1996.
- G. M. Sheldrick, *SHELXS-97, Program for solution of crystal structures*, University of Göttingen, Germany, 1997;

- G. M. Sheldrick, *SHELXL-97, Program for refinement of crystal structures*, University of Göttingen, Germany, 1997.
- 31 A. L. J. Spek, *Appl. Crystallogr.*, 2003, **36**, 7–13.
- 32 R. Janes and E. A. Moore, in *Metal-ligand Bonding*, ed. E. W. Abel, Royal Society of Chemistry, Cambridge, UK, 2004.
- 33 A. Blatov, *IUCr CompComm Newslett.*, 2006, vol. 7, p. 4, TOPOS is available at <http://www.topos.ssu.samara.ru/>.
- 34 J. Mukherjee and R. Mukherjee, *Inorg. Chim. Acta*, 2002, **337**, 429–438.
- 35 C. G. Pierpont, *Coord. Chem. Rev.*, 2001, **216–217**, 99–125.
- 36 O.-S. Jung, D. H. Jo, Y.-A. Lee, B. J. Conklin and C. G. Pierpont, *Inorg. Chem.*, 1997, **36**, 19–24.
- 37 P. A. Wicklund and D. G. Brown, *Inorg. Chem.*, 1976, **15**, 396–400.
- 38 M. D. Stallings, M. M. Morrison and D. T. Sawyer, *Inorg. Chem.*, 1981, **20**, 2655–2660.
- 39 V. K. Bhardwaj, N. Aliaga-Alcalde, M. Corbella and G. Hundal, *Inorg. Chim. Acta*, 2010, **363**, 97–106.
- 40 H. Lee, T. H. Noh and O.-S. Jung, *Chem. Commun.*, 2013, **49**, 9182–9184.
- 41 T. Klabunde, C. Eicken, J. C. Sacchettini and B. Krebs, *Nat. Struct. Biol.*, 1998, **5**, 1084–1090.
- 42 S. E. Allen, R. R. Walvoord, R. Padilla-Salinas and M. C. Kozłowski, *Chem. Rev.*, 2013, **113**, 6234–6458.
- 43 E. I. Solomon, D. E. Heppner, E. M. Johnston, J. W. Ginsbach, J. Cirera, M. Qayyum, M. T. Kieber-Emmons, C. H. Kjaergaard, R. G. Hadt and L. Tian, *Chem. Rev.*, 2014, **114**, 3659–3853.